

Lateral imaging of the superconducting vortex lattice using Doppler-modulated scanning tunneling microscopy

I. Fridman,¹ C. Kloc,² C. Petrovic,³ and J. Y. T. Wei^{1,4}

¹Department of Physics, University of Toronto, 60 St. George St., Toronto ON M5S1A7 Canada

²School of Materials Science and Engineering, Nanyang Technological University 639798 Singapore

³Condensed Matter Physics and Materials Science Department, Brookhaven National Laboratory, Upton, NY 11973 USA

⁴Canadian Institute for Advanced Research, Toronto, ON, M5G1Z8 Canada

By spatially mapping the Doppler effect of an in-plane magnetic field on the quasiparticle tunneling spectrum, we have laterally imaged the vortex lattice in superconducting $2H\text{-NbSe}_2$. Cryomagnetic scanning tunneling spectroscopy was performed at 300 mK on the ab -surface oriented parallel to the field H . Conductance images at zero bias show stripe patterns running along H , with the stripe separation varying as $H^{-0.5}$. Regions of higher zero-bias conductance show lower gap-edge conductance, consistent with spectral redistribution by spatially-modulated superfluid momentum. Our results are interpreted in terms of the interaction between vortical and screening currents, and demonstrate a general method for probing subsurface vortices.

PACS numbers: 74.55.+v, 74.25.Uv, 74.70.Ad

In response to an applied magnetic field, type-II superconductors experience a diamagnetic current that circulates along the sample edge. Above the lower critical field, field can penetrate into the superconductor via a lattice of vortices, each consisting of a paramagnetic current loop enclosing a flux quantum.¹ The vortex lattice can be imaged using techniques sensitive to variations in the local magnetic field such as Bitter decoration² and Lorentz microscopy,³ or with scanning tunneling microscopy (STM) which probes the local quasiparticle density of states (DOS). STM imaging of the vortices is possible by virtue of bound states and suppressed superconducting gap in the vortex core.^{4,5} Because of this reliance on vortex-core states, STM imaging has been largely limited to the cross-sectional geometry, i.e. with the vortices piercing the sample surface. An earlier STM study versus field direction has shown the density of vortices to decrease as the field is tilted away from the surface normal.^{6,7} For fields parallel to the surface, the vortex cores become buried in the bulk, making them difficult to probe directly. In this lateral field geometry, vortex lattices have been imaged by Lorentz microscopy, but only in highly 2D superconductors where pancake vortices decorate in-plane flux lines.^{8,9}

In this letter, we report on lateral imaging of the superconducting vortex lattice using cryomagnetic scanning tunneling spectroscopy. By mapping the zero-bias tunneling conductance over the ab -surface of superconducting $2H\text{-NbSe}_2$ in an in-plane magnetic field and at 300 mK, we have observed distinct stripe patterns whose orientation and spacing versus the field can be directly attributed to the in-plane flux lattice. Our observations are interpreted in terms of the interaction between the diamagnetic screening current and the paramagnetic vortical currents, which results in a spatially-modulated Doppler effect on the quasiparticle DOS spectrum.

The STM used in our experiment was specially designed for the magnetic field to be applied parallel to the sample surface, as shown in Fig. 1(e). The STM

is mounted inside a ^3He cryostat which is inserted into a superconducting solenoid. The Pt-Ir tips used were field-emitted *in situ* to ensure stable vacuum tunneling, and RF-filters were used throughout the wiring to maximize the spectral resolution. The dI/dV conductance spectra were acquired by lock-in amplification with a 20 μV

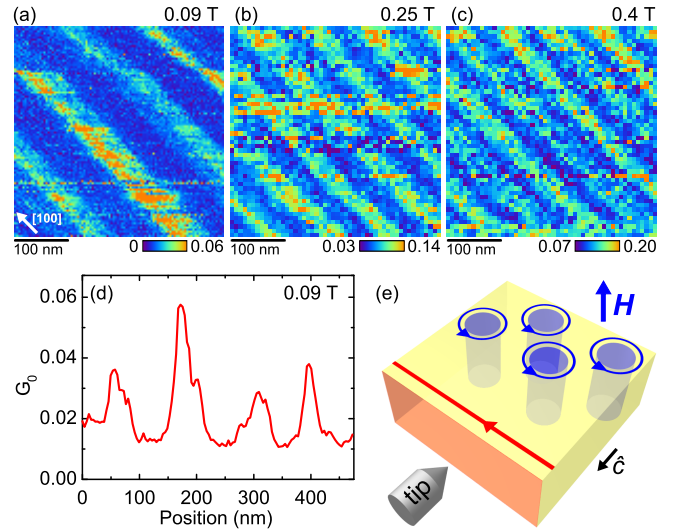


FIG. 1. Lateral imaging of the superconducting vortex lattice in $2H\text{-NbSe}_2$ at various fields and 300 mK. Panels (a) to (c) show $380 \times 380 \text{ nm}^2$ spatial maps of the normalized zero-bias tunneling conductance G_0 for fields of 0.09 T, 0.25 T, and 0.4 T, applied along the $[100]$ direction (white arrow in (a)). Panel (d) shows the average G_0 along the direction perpendicular to the stripes in the 0.09 T data. Panel (e) shows a schematic of our experiment, with the STM measuring the ab -surface, across which flows a diamagnetic screening current (red line). In the heuristic model discussed in the text, paramagnetic currents (blue loops) circulating the subsurface vortices perturb the screening current, thus spatially modulating G_0 and producing the observed G_0 image contrast.

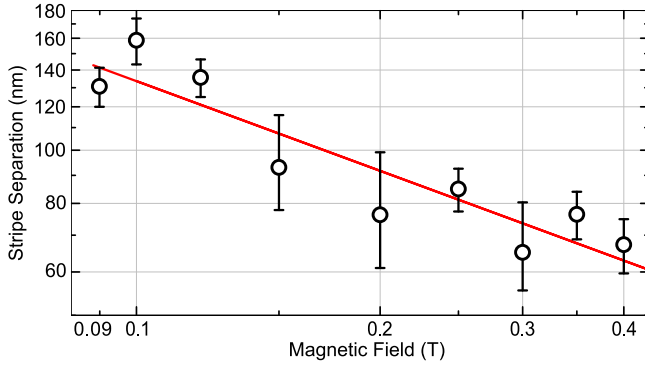


FIG. 2. Separation between the centers of the G_0 stripes, for fields between 0.09 T and 0.4 T, plotted on a log-log scale. The data (circles) are fitted to $\propto H^{-0.54 \pm 0.09}$ (red line), in good agreement with the expected $H^{-0.5}$ dependence of the vortex lattice parameter on field.

excitation at 505 Hz, and the typical high-bias junction impedance was 10 M Ω .

Single crystals of $2H\text{-NbSe}_2$ were grown by an iodine vapor transport technique.¹⁰ The crystals had critical temperatures of ≈ 7.2 K, and upper critical fields of ≈ 5 T and 15 T respectively for field perpendicular and parallel to the ab -plane. The crystals measured were $\sim 5 \times 5 \times 0.5$ mm³ in size, with the wide faces normal to the c -axis. The crystals were oriented by X-ray diffraction, cleaved just before being loaded into the STM and cooled to 300 mK in zero field. STM topography revealed atomically smooth surfaces, with hexagonally arranged Se atoms modulated by triangular charge density waves. The magnetic field was applied along the [100] direction with $\sim 2^\circ$ precision.

Figure 1 shows spatial maps of the zero-bias conductance, G_0 . The G_0 data was normalized relative to the above-gap conductance at 4 mV. Panels (a) to (c) show plots of the data for 0.09 T, 0.25 T and 0.4 T respectively. Regions of high G_0 , hereafter referred to as stripes, can be seen in each plot, running parallel to the in-plane field and spaced at regular intervals. Crystals from different growth batches showed the same stripe patterns, thus attesting to their general reproducibility. The average half-width of the stripes is 35 ± 15 nm over the field range measured. This is comparable to the expected size of a vortex core $2\xi_{ab} \sim 20$ nm, where ξ_{ab} is the zero-temperature superconducting coherence length in the ab -plane for $2H\text{-NbSe}_2$.¹¹ The brightness of the stripes alternates between adjacent stripes, an effect more clearly seen in panel (d), which shows a profile plot of the average G_0 along the direction perpendicular to the stripes in the 0.09 T data.

To interpret the stripe patterns as a manifestation of the subsurface flux vortices, we consider quantitatively how these patterns vary with the applied field H . Figure 2 shows a log-log plot of the separation between stripe centers over the field range measured in this experiment. The stripe separation decreases with increasing field and is fitted to $\propto H^{-0.54 \pm 0.09}$, in good agreement with the

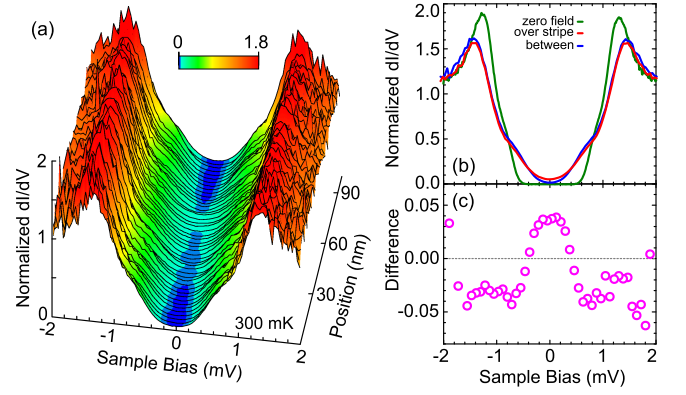


FIG. 3. (a) Series of normalized dI/dV spectra measured as the tip is scanned perpendicularly across a stripe at 0.1 T and 300 mK. The midgap states rise over a ≈ 35 nm wide region, thus accounting for the stripe patterns seen in the G_0 images. (b) Spatially-averaged dI/dV spectra over the center of a stripe (red curve) and just between two stripes (blue curve). The zero-field spectrum (green curve) is included for comparison, to show the overall effect of the applied field. Over the stripe, the zero-bias dI/dV is higher while the coherence-peak dI/dV is lower, an effect clearly seen in the difference of the two curves, as shown in (c).

expected $H^{-0.5}$ dependence of the vortex lattice parameter on field. It is important to note that the stripe separation we observed is 0.86 ± 0.10 times the Abrikosov lattice parameter. This observation can be qualitatively explained by identifying every other stripe with the row of flux lines closest to the surface, and the in-between stripes as coming from the next closest row; this picture would be consistent with the alternating brightness between adjacent stripes noted above. A more quantitative explanation of the stripe separation observed would need to consider vortex lattice distortions due to the superconducting anisotropy of $2H\text{-NbSe}_2$ over the field range we measured.¹²

To visualize spectroscopically how the stripe patterns emerge, we analyze detailed variations in the dI/dV spectrum across a typical G_0 image. Figure 3(a) shows a series of dI/dV spectra measured while the tip is scanned perpendicularly across a stripe region at 0.1 T. It is clear that the midgap states rise appreciably over a ≈ 35 nm wide region, thus accounting for the stripe patterns seen in the G_0 image described above. Panel (b) shows the spatially-averaged spectra over the center of a stripe and just between two stripes. The zero-field spectrum is included for comparison, to show the overall effect of the applied field. Comparing the two curves at 0.1 T, the zero-bias dI/dV is higher while the dI/dV near the coherence peak at $\approx \pm 1.4$ mV is lower, over a stripe than between stripes. This effect can be seen more clearly in the difference of the two spectra, as shown in panel (c). Here we emphasize the subtlety of this midgap-states effect, i.e. the difference in G_0 is ≈ 5 nS, requiring high measurement sensitivity to detect.

To understand the physical origin of the spectral evolution versus field, we consider the recent theoretical model of Zhang *et al.* (Ref. 13), which calculates the quasiparticle DOS spectrum for a current-carrying superconductor. Essentially, the supercurrent adds a Doppler term proportional to $\mathbf{v}_F \cdot \mathbf{q}_s$ to the quasiparticle energy dispersion E_k , where \mathbf{v}_F is the Fermi velocity and \mathbf{q}_s is the superfluid momentum. This Doppler shift in k -space causes a redistribution of the energy-gap size along the Fermi surface (FS), thus modifying the quasiparticle DOS spectrum.¹⁴ With increasing \mathbf{q}_s , the coherence peaks are suppressed in height and shifted to higher energies.^{13,15} When the Doppler term becomes sufficiently large relative to the gap amplitude, parts of the FS become gapless, causing the zero-energy DOS to increase with the field. All of these spectral behaviors, namely suppression of the coherence peak and enhancement of the midgap states, are observed in our tunneling measurements, thus directly implicating the Doppler effect in the appearance of finite G_0 with in-plane field.

Finally, we consider the interaction between the vortical and screening currents, in order to explain why the Doppler redistribution of the quasiparticle DOS spectrum shows spatial modulation that is correlated with the vortex lattice. These two currents flow in opposite directions near the sample surface, as shown in Fig. 1(e), and the counter-flowing current lines would be denser over certain regions in order to avoid crossing each other, thereby locally enhancing the supercurrent density and thus the superfluid momentum. A spatially-modulated superfluid momentum implies a spatially-modulated Doppler effect, which could then produce the stripe patterns seen in our in-field STM measurements. In this heuristic model, the stripes in the G_0 image corresponding to high-Doppler regions are over vortices, while the spaces between stripes corresponding to low-Doppler regions are between vortices. Although this model is physically plausible, it should be noted that there are alternative models indicating the opposite scenario, i.e. larger current density and thus stronger Doppler effect between vortices than over vortices.^{16,17} Applicabilities of these models depend on quantitative details of the model assumptions, in particular the field strength relative to the thermodynamic critical field and the coherence length relative to the London penetration depth. Further theoretical work is needed to more rigorously justify our model and quantitatively interpret our data. Here it is also worth noting that the subgap features at $\approx \pm 0.7$ mV seen in our spectra could be due to the multiband nature of 2H-NbSe₂, as manifestations of a smaller superconducting energy gap which is also Doppler-redistributed by the in-plane field.^{18–21} Elucidation of this scenario would require a multiband generalization of the Zhang *et al.* model.¹³, but would not affect the stripe patterns

we observed or our interpretation of their physical origin.

In summary, we have used Doppler-modulated scanning tunneling microscopy, performed at 300 mK, to laterally image the in-plane vortex lattice in superconducting 2H-NbSe₂. This technique can in principle be applied on various other superconductors to probe the length scales and spatial symmetry of subsurface flux vortices. It may also potentially be used to study other fundamental vortex phenomena, such as single-vortex entry and vortex-surface interactions.

We acknowledge useful discussions with J. R. Clem, C.-R. Hu, V. G. Kogan and A. Paramakanti. This work was supported by NSERC, CFI-OIT and the Canadian Institute for Advanced Research. Part of this work was carried out at BNL, which is operated for the U.S. Department of Energy by Brookhaven Science Associates (Grant No. DE-Ac02-98CH10886).

- ¹A. A. Abrikosov, Sov. Phys. JETP **5**, 1174 (1957).
- ²U. Essmann and H. Truble, Phys. Lett. A **24**, 526 (1967).
- ³T. Matsuda, O. Kamimura, H. Kasai, K. Harada, T. Yoshida, T. Akashi, A. Tonomura, Y. Nakayama, J. Shimoyama, K. Kishio, T. Hanaguri, and K. Kitazawa, Science **294**, 2136 (2001).
- ⁴C. Caroli, P. G. D. Gennes, and J. Matricon, Phys. Lett. **9**, 307 (1964).
- ⁵H. F. Hess, R. B. Robinson, R. C. Dynes, J. M. Valles, and J. V. Waszczak, Phys. Rev. Lett. **62**, 214 (1989).
- ⁶H. F. Hess, C. A. Murray, and J. V. Waszczak, Phys. Rev. Lett. **69**, 2138 (1992).
- ⁷H. F. Hess, C. A. Murray, and J. V. Waszczak, Phys. Rev. B **50**, 16528 (1994).
- ⁸V. K. Vlasko-Vlasov, A. Koshelev, U. Welp, G. W. Crabtree, and K. Kadowaki, Phys. Rev. B **66**, 014523 (2002).
- ⁹M. Yasugaki, K. Itaka, M. Tokunaga, N. Kameda, and T. Tamegai, Phys. Rev. B **65**, 212502 (2002).
- ¹⁰C. S. Oglesby, E. Bucher, C. Kloc, and H. Hohl, Journal of Crystal Growth **137**, 289 (1994).
- ¹¹F. D. Callaghan, M. Laulajainen, C. V. Kaiser, and J. E. Sonier, Phys. Rev. Lett. **95**, 197001 (2005).
- ¹²L. J. Campbell, M. M. Doria, and V. G. Kogan, Phys. Rev. B **38**, 2439 (1988).
- ¹³D. Zhang, C. S. Ting, and C.-R. Hu, Phys. Rev. B **70**, 172508 (2004).
- ¹⁴P. Fulde, in *Tunneling Phenomena in Solids*, edited by E. Burstein and S. Lundqvist (Plenum, New York, 1969) p. 427.
- ¹⁵A. Kohen, T. Proslir, T. Cren, Y. Noat, W. Sacks, H. Berger, and D. Roditchev, Phys. Rev. Lett. **97**, 027001 (2006).
- ¹⁶E. H. Brandt, Journal of Low Temperature Physics **42**, 557 (1981).
- ¹⁷A. D. Hernández and A. López, Phys. Rev. B **77**, 144506 (2008).
- ¹⁸E. Boaknin, M. A. Tanatar, J. Paglione, D. Hawthorn, F. Ronning, R. W. Hill, M. Sutherland, L. Taillefer, J. Sonier, S. M. Hayden, and J. W. Brill, Phys. Rev. Lett. **90**, 117003 (2003).
- ¹⁹C. L. Huang, J.-Y. Lin, Y. T. Chang, C. P. Sun, H. Y. Shen, C. C. Chou, H. Berger, T. K. Lee, and H. D. Yang, Phys. Rev. B **76**, 212504 (2007).
- ²⁰J. G. Rodrigo and S. Vieira, Physica C: Superconductivity **404**, 306 (2004).
- ²¹I. Guillamon, H. Suderow, F. Guinea, and S. Vieira, Phys. Rev. B **77**, 134505 (2008).